Nano Research

Open Access

Research Article

A series of tetraphenylethylene-pyridine derivatives with multi-site substitutions for fluorescence nanoparticles: Structure-fluorescence relationship, pH-sensitivity, drug delivery and anti-tumor effect

Zengfang Huang[1,2] ✉, Jinwen Tan[1,2], Siying Yang[1], Weicheng Zhou[1], Juntao Zhang[1], Yang Yang[4], Mei Tian[5], Jinying Yuan[3], Lei Tao[3], and Yen Wei[3] ✉

[1] *Zhongshan Institute, University of Electronic Science & Technology of China, Zhongshan 528402, China*
[2] *School of Materials and Energy, University of Electronic Science & Technology of China, Chengdu 610054, China*
[3] *The Key Laboratory of Bioorganic Phosphorus Chemistry & Chemical Biology (Ministry of Education), Department of Chemistry, Tsinghua University, Beijing 100084, China*
[4] *Institute of Nuclear and New Energy Technology, Tsinghua University, Beijing 100084, China*
[5] *Human Phenome Institute, Fudan University, 825 Zhangheng Road, Shanghai 201203, China*

Cite this article: *Nano Research*, **2026**, *19*, 94908481. https://doi.org/10.26599/NR.2026.94908481

ABSTRACT: The development of drug delivery systems with good biocompatibility, stability, fluorescence sensors and targeting capability is of great importance in biomedical research. In this work, we present the first systematic investigation of various site substitution effects on a series of fluorescent materials with aggregation-induced emission (AIE) characteristics. Thus, AIE active triphenylvinyl-benzaldehyde (TPB) and triphenylvinylphenylpyridine (TPE-PY) derivatives with various aldehyde and pyridine positions were prepared via McMurry, Sonogashira and Suzuki reactions. As compared with TPB derivatives, TPE-PY derivatives showed significant changes in emission wavelength and intensity, displaying typical AIE behavior, longer wavelength emission, and pH-responsivity. Quantum chemical calculations also confirmed lower energy bandgaps (ΔE) of TPE-PY derivatives, in which TPE-PPY have the lowest ΔE (2.98 eV) due to extended conjugation effect. Considering the redshift and good fluorescence emission of TPE-4PY, DPT-4PY fluorescent organic nanoparticles (FONs) were prepared via physical encapsulation with amphiphilic DSPE-PEG2000, which exhibited excellent biocompatibility, low toxicity, and good potential for bioimaging applications. Furthermore, since TPE-PPY exhibited optimal fluorescence performance, a novel fluorescent monomer divinylbenzene-pyridin-acrylonitrile (DVBPA) with AIE characteristics was synthesized for the amphiphilic copolymer PEG-BPA from reversible addition-fragmentation chain-transfer (RAFT) polymerization, which would self-assemble to form nanoparticles about 100–200 nm in water solution. PEG-BPA FONs demonstrated superior fluorescence stability, biocompatibility, and cellular uptake, enabling their application as carriers of paclitaxel (PTX) to construct BPA-PTX FONs drug delivery system for anti-tumors effect. The drug-loaded nanoparticles exhibited high encapsulation efficiency, loading capacity, and significant A549 cells inhibition. This nano system is promising for applications in bioimaging, drug delivery, tumors microenvironment sensing, and anti-tumors therapy.

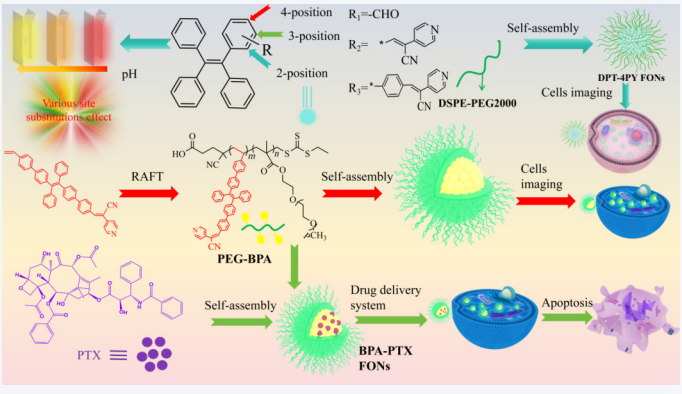

KEYWORDS: multi-site substitutions, aggregation-induced emission (AIE), pH-sensitivity, cell imaging, drug delivery

Received: December 17, 2025; **Revised:** January 20, 2026
Accepted: January 21, 2026

✉Address correspondence to Zengfang Huang, hzf105@163.com; Yen Wei, weiyen@tsinghua.edu.cn

1 Introduction

Owing to their excellent optical properties, fluorescent materials have emerged as essential components in broad biomedical applications of cell imaging, diagnostic techniques, and targeted drug delivery, etc. Integrating fluorescent materials with medicine

enables real-time monitoring of intracellular molecular dynamics, it provides critical information for early disease detection and treatment evaluation [1–3]. However, traditional fluorescent materials frequently suffer from aggregation-caused quenching (ACQ) at high concentrations or in aggregated states [4], which significantly reduces their fluorescence intensity and limits their application in biomedical fields. In biological environments, fluorophores will aggregate due to the high local concentrations or interactions with biomolecules to cause quenching and reduce imaging sensitivity and accuracy. To overcome the ACQ effect, aggregation-induced emission (AIE) materials have been developed, exhibiting enhanced fluorescence intensity in the aggregated state. Unlike conventional fluorescent materials, AIE materials show negligible fluorescence in dilute solutions but emit strong fluorescence in aggregated states, offering excellent photostability and biocompatibility [5–9]. These properties make AIE materials be promising candidates for bioimaging, cancer diagnosis, and drug delivery [10–12]. Many AIE molecules, such as tetraphenylethylene (TPE), carbazole (CZ), and thiophene (TPA), have been widely used in biomedical applications [13–20]. To enhance the specific responsiveness of AIE materials in biological environments, pH-responsive systems have gained increasing attention due to their strong relevance to the acidic nature of the tumor microenvironment [21–24]. In such conditions, pH-sensitive AIE materials can undergo conformations or charges state changes at various pH, thereby triggering fluorescence signal variations or enabling controlled drug release for targeted therapy and real-time monitoring. A pH-sensitive TPE probe was prepared by molecular design, showing dual-channel imaging of viscosity and pH during drug treatment, enabling selective visualization of cancer cells and tissues [25]. These materials not only retain AIE properties but also precisely respond to microenvironmental changes, improving the accuracy and efficacy of biomedical applications.

As a broad-spectrum anticancer drug, paclitaxel (PTX) has been extensively used to treat solid tumors such as breast, ovarian, and lung cancers, because it can inhibit microtubule depolymerization, causing cell cycle arrest and apoptosis [26]. However, PTX suffers from low water solubility and rapid clearance, limiting its therapeutic efficacy [27]. To address these challenges, nanocarriers have been developed to enhance the bioavailability of PTX and achieve targeted drug delivery. A two-photon red-emissive AIE molecule was designed and synthesized to construct an AIE@PTX nanoparticle system, which exhibited efficient tumor targeting, strong antitumor efficacy, and good biocompatibility [28]. A novel copolymer (CD-CS-Bio-TPAA, CCBT) was fabricated, which can self-assemble into polymeric micelles and serve as a drug carrier for encapsulating PTX (PTX/CCBT PMs), enabling self-indicating cancer therapy [24].

In this study, in order to better understand the effect of substitution positions on fluorescence performance due to the conjugation effect for the electron cloud shift, a series of small molecules TPB and pH-sensitive TPE-PY were synthesized with tetraphenylethylene, nitrile and pyridine groups as shown in Scheme 1, and DPT-4PY FONs showed the promising the cells imaging via physical encapsulation of TPE-4PY with amphiphilic distearylphosphatidylethanolamine-polyethylene glycol (DSPE-PEG2000). As far as we know, this is the first systematic investigation of various site substitution effects on a series of fluorescent materials with AIE characteristics. Quantum chemical calculations confirmed low energy bandgaps (ΔE) for TPE-PY derivatives, with TPE-PPY having the lowest value due to extended conjugation. Subsequently, the key intermediates bromophenyl-diphenylvinyl-carbaldehyde (BDBC) and diphenylvinyl-biphenylcarbaldehyde (DVBC) were constructed for the design and synthesis of fluorescent monomer divinylbenzene-pyridin-acrylonitrile (DVBPA), which was used for the amphiphilic copolymers PEG-BPA by reversible addition-fragmentation chain-transfer (RAFT) polymerization. Notably, the introduction of a pyridine group in place of the aldehyde moiety effectively red-shifted the emission wavelength, enhancing fluorescence in the visible region and making the materials more suitable for biological imaging. Considering the acidity of the tumor microenvironment, pH-sensitive BPA-PTX FONs was constructed from the self-assembly of PEG-BPA copolymers and anti-tumors drug PTX for the PTX drug release and delivery in the tumors cells A549, which not only elucidates the structure-property relationship from small molecules to polymers, but also demonstrates the potential of this AIE-based multifunctional platform in bioimaging, drug delivery, and cancer therapy, in order to provide new insights and strategies for the development of smart nanocarriers based on AIE materials.

2 Experimental

2.1 Materials and characterization

Poly(ethylene glycol) methacrylate (PEGMA, Aladdin, M_n = 475, analytical reagent purity (AR)), chains transfer agent (CTA) of 4-cyano-4-(ethylthiocarbonylthiothiothiothio) pentanoic acid, and 1,2-bis(4-bromophenyl)-1,2-diphenylethene (BBrDP) were respectively refined and synthesized by the previous reported method [19, 29, 30],

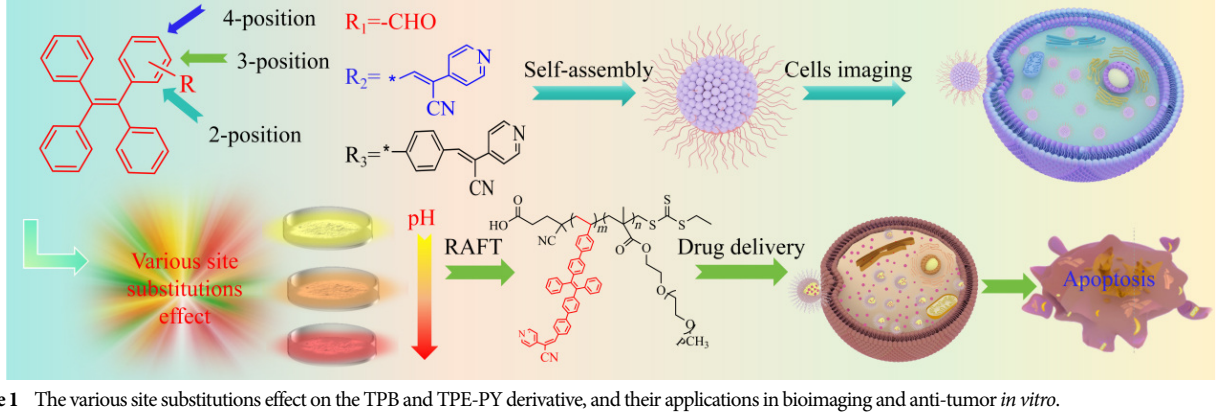

Scheme 1 The various site substitutions effect on the TPB and TPE-PY derivative, and their applications in bioimaging and anti-tumor *in vitro*.

and other materials and characterization methods are referred to in the Electronic Supplementary Material (ESM).

2.2 Synthesis of TPB, TPE-PY, DVBPA monomers and their copolymers PEG-BPA

The detailed synthetic procedures for TPB derivatives (2-TPB, 3-TPB, 4-TPB, 4-TPPB) and TPE-PY derivatives (TPE-2PY, TPE-3PY, TPE-4PY, TPE-PPY) together with their mass spectra of Figs. S1–S4 are shown in the ESM and related literature [31], the synthesis of intermediates BDBC and DVBC, DVBPA monomers together with their mass spectra of Figs. S5–S7 is in the ESM, and the fabrication of corresponding copolymers PEG-BPA and their self-assembly systems DPT-4PY FONs and BPA-PTX FONs are also in the ESM.

3 Results and discussion

3.1 Synthesis and photophysical properties of TPE-PY and copolymers PEG-BPA

Synthetic strategies of TPB and TPE-PY derivatives with different positions of aldehyde and pyridine groups are illustrated in Scheme 2 together with DVBPA monomers and PEG-BPA copolymers. Firstly, TPB derivatives were synthesized via Suzuki coupling reactions between BrTPE and the corresponding fluorophenylboronic acid (FPBA) in toluene solution with $Pd(PPh_3)_4$ as catalysis. TPB would undergo Sonogashira coupling reactions with 2-(pyridin-4-yl)acetonitrile to yield the corresponding TPE-PY with pH-responsive properties. Subsequently, DPT-4PY FONs were fabricated through the physical encapsulation of TPE-4PY by DSPE-PEG2000 for the cellular imaging applications. Given the pH sensitivity and potential red-shifted emission of TPE-PY derivatives, TPE-PPY was further selected as the basic structure for the synthesis of DVBPA monomers. The reaction process of DVBPA monomers involved four main steps. Initially, McMurry coupling was used to synthesize the intermediate BBrDP from (4-bromobenzene)(phenyl)methanone (4-BrBPM), $TiCl_4$, zinc powder, and tetrahydrofuran (THF) [32], and then the aldehyde intermediate BDBC was synthesized via the Suzuki coupling reaction of BBrDP and 4-formylphenylboronic acid with $Pd(PPh_3)_4$ as catalysis. Next, BDBC underwent Suzuki coupling with 4-vinylphenylboronic acid to produce the monomers DVBC. Finally, DVBC reacted with 4-pyridine acetonitrile in a Sonogashira coupling reaction to form DVBPA through the connection of the pyridyl with AIE backbone. The amphiphilic copolymer PEG-BPA was synthesized by the RAFT polymerization of the DVBPA monomer and PEGMA. The incorporation of hydrophobic DVBPA and hydrophilic PEGMA enables the copolymer to self-assemble into PEG-BPA FONs in aqueous solution, making them suitable for cell imaging. Leveraging its amphiphilic core-shell architecture, these nanoparticles can also be used for load of the anticancer drug PTX to form BPA-PTX FONs for drug delivery system.

The gel permeation chromatography (GPC) curves of PEG-BPA1 and PEG-BPA2 are presented in Fig. 1(a) with the ^{1}H nuclear magnetic resonance (NMR) spectra of TPB and TPE-PY derivatives, monomer DVBPA and the copolymer PEG-BPA1. In Fig. 1(a), PEG-BPA1 exhibits a molecular weight (Mw) of 1.41×10^4 with polydispersity index (PDI) of 1.23, while PEG-BPA2 has an Mw of 1.23×10^4 and a PDI of 1.25. The similar and relatively narrow PDI values indicated the good controllability of PEG-BPA copolymers via the RAFT polymerization process.

As illustrated in Fig. 1(b), the absorption peaks of TPB are predominantly observed at 6.95–7.93 ppm of the aromatic region

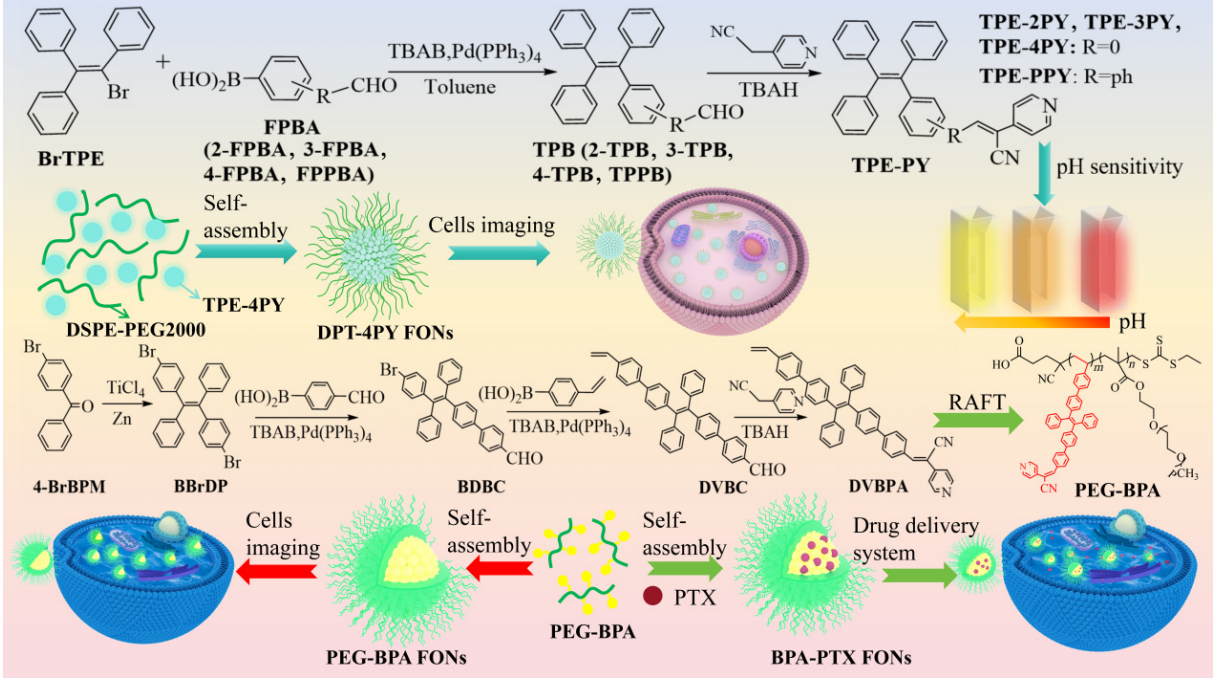

Scheme 2 The synthetic routes of fluorescent compounds TPE-2PY, TPE-3PY, TPE-4PY, and TPE-PPY were designed for investigating structure-activity relationships and pH sensitivity; DPT-4PY FONs were fabricated by the self-assembly of TPE-4PY with hydrophilic DSPE-PEG2000 for cellular imaging; PEG-BPA copolymers were prepared by RAFT polymerization, which further self-assembled into fluorescent nanoparticles for imaging and encapsulating PTX to form BPA-PTX FONs for drug delivery system.

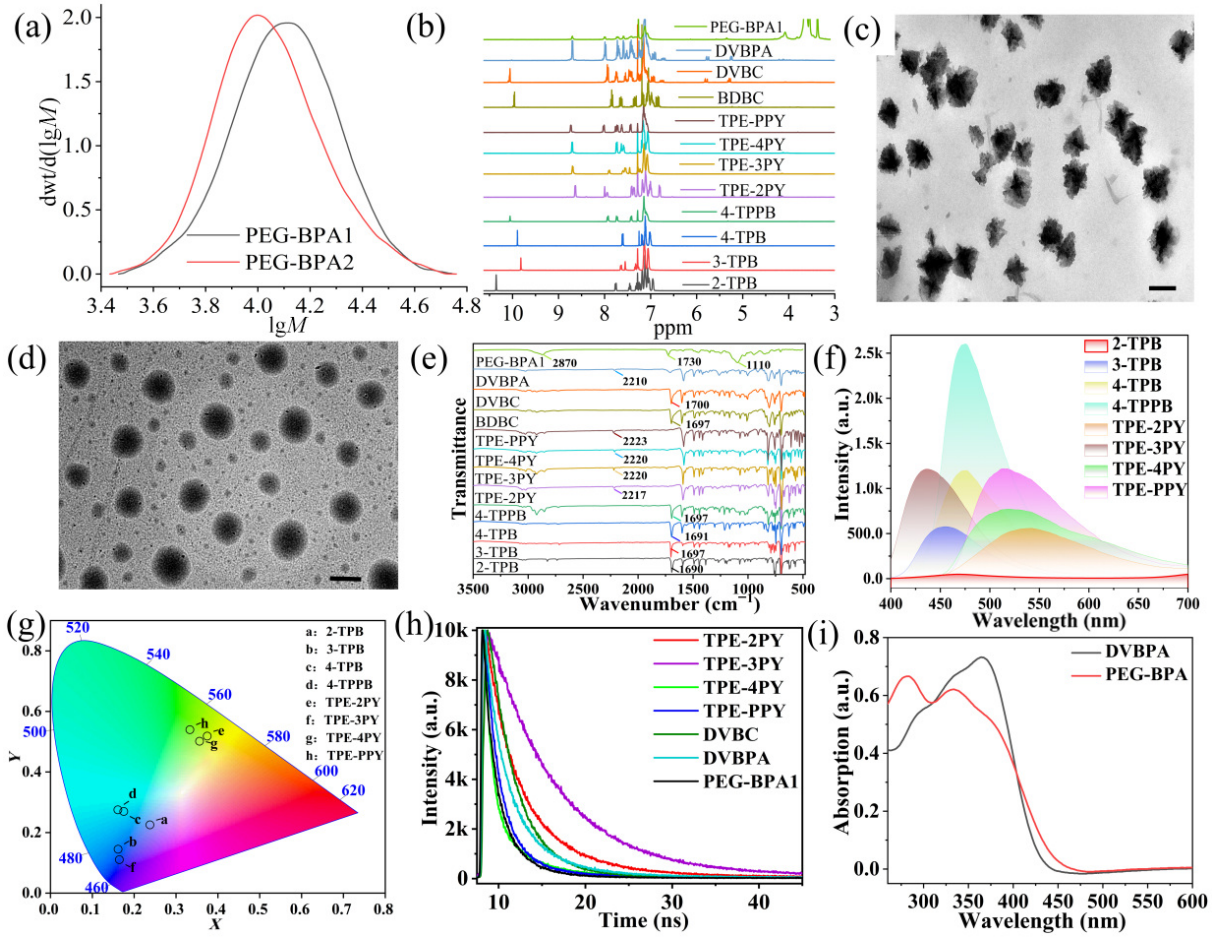

Figure 1 (a) GPC curves of PEG-BPA copolymers (PEG-BPA1, M_W = 1.41 × 10⁴, PDI = 1.23; PEG-BPA2, M_W = 1.23 × 10⁴, PDI = 1.25). (b) ^{1}H-NMR spectra ($CDCl_3$) of fluorescence compounds TPB, TPE-PY derivatives, key intermediate BDBC, DVBC, monomers DVBPA and copolymers PEG-BPA. (c) TEM image of DPT-4PY FONs dispersed in H_2O (scale bar = 200 nm). (d) TEM image of PEG-BPA1 FONs dispersed in H_2O (scale bar = 200 nm). (e) FTIR spectra of fluorescent compounds TPB, TPE-PY, key intermediate BDBC, DVBC, monomer DVBPA, and PEG-BPA1 copolymer. (f) Fluorescence emission spectra of TPB and TPE-PY. (g) CIE of TPB and TPE-PY. (h) Fluorescence decay curves of TPE-2PY (τ_1 = 2.82, τ_2 = 6.75, χ = 1.06), TPE-3PY (τ_1 = 7.73, χ = 1.16), TPE-4PY (τ_1 = 0.92, τ_2 = 4.86, χ = 1.42), TPE-PPY (τ_1 = 1.71, τ_2 = 5.97, χ = 1.23), DVBC (τ_1 = 3.27, χ = 1.89), DVBPA (τ_1 = 2.22, τ_2 = 5.64, χ = 1.06) fluorescence copolymers PEG-BPA1 (τ_1 = 1.40, τ_2 =3.68, χ = 1.20). (i) Ultraviolet–visible (UV–Vis) absorption characteristics of DPBPA monomer in THF and PEG-BPA1 copolymer in water.

with an additional distinct peak at 10.00 ppm corresponding to the –CHO. In comparison to TPB, the corresponding TPE-PY compounds exhibit the disappearance of the absorption peak at 10.00 ppm, and a new characteristic peak emerges at about 8.70 ppm, which indicates that the aldehyde group has been disappeared and the pyridine group was successfully introduced into. For BDBC, the proton signals of –CHO group appear at 9.97 ppm, implying the successful incorporation of benzaldehyde, moreover, the obvious peaks in DVBC spectra are observed at 5.25, 5.76, and 6.93 ppm with 1:1:1 integral ratio, indicative of the expected introduction of styrene ingredients. As compared with DVBC, the spectrum of the DVBPA monomer exhibits a new peak at 8.70 ppm assigning to the pyridine group, along with the disappearance of the aldehyde proton signal at 9.97 ppm, confirming the successful formation of DVBPA. For the PEG-BPA1 copolymers, the characteristic absorption peaks corresponding to DVBPA at 5.25, 5.76, and 6.93 ppm were entirely absent, concurrently, the emergence of the characteristic absorption peak of PEGMA at 4.07 ppm demonstrated the successful integration of DVBPA and PEGMA into the PEG-BPA copolymer via RAFT polymerization.

In order to investigate the self-assembly morphology of DPT-4PY FONs and PEG-BPA1 FONs, their TEM images from aqueous solution are respectively shown in Figs. 1(c) and 1(d). As shown in Fig. 1(c), TPE-4PY was physically encapsulated by the amphiphilic block molecules DSPE-PEG2000 to form DPT-4PY FONs with a diameter of approximately 200 nm, where a distinct biphasic structure can be observed with TPE-4PY as the core and DSPE-PEG2000 as the shell. Meanwhile, in the PEG-BPA1 copolymers as shown in Fig. 1(d), the hydrophilic PEGMA segments extend into the aqueous phase, while the hydrophobic DVBPA segments aggregate and are encapsulated within the core, leading to the spontaneous formation of core-shell nanoparticles with DVBPA as the core and PEGMA as the shell. As compared with DPT-4PY FONs, the PEG-BPA1 FONs exhibit a uniform spherical morphology with diameters of approximately 100–200 nm, which is more suitable for cellular uptake and imaging applications.

Figure 1(e) further illustrates the Fourier transform infrared spectroscopy (FTIR) spectra of TPB, TPE-PY derivatives, intermediate BDBC, DVBC, monomer DVBPA, and the copolymer PEG-BPA1. The FTIR spectra of TPB derivatives, BDBC, and DVBC show characteristic peaks at 1690–1700 cm^{-1}

attributing to the C=O stretching vibrations of aldehyde groups, confirming their successful incorporation. For TPE-PY and DVBPA, the disappearance of the stretching vibration peak at 1690–1700 cm^{-1}, along with the appearance of a new peak at 2217–2223 cm^{-1} corresponding to the –C≡N group, indicative of the successful incorporation of the pyridine moiety via the Sonogashira coupling reaction. For the FTIR spectrum of the PEG-BPA copolymers, three distinct absorption peaks appear at 2870, 1730, and 1110 cm^{-1} corresponding to the $–CH_2–$, –C=O, and –C–O– groups from the DVBPA and PEGMA segments, respectively, confirming the successful synthesis of the PEG-BPA copolymers.

The fluorescence emission spectra and decay curves are shown in Figs. 1(f)–1(h) to reveal the optical properties of the synthesized DVBPA monomer and PEG-BPA copolymer, as well as the structure-property relationships of TPB and TPE-PY derivatives. Through the detailed interpretation of the spectra of Fig. 1(f) for the difference of optical properties between the TPB and TPE-PY series, we can deeply understand how the molecular structure can precisely regulate its luminescence behavior through substitution sites, conjugation effects and electronic effects. TPB compounds are a class of molecules with 1,2,2-tristyrene as the core skeleton, and their optical properties can be adjusted by the position of benzaldehyde substituents. As the substitution site shifts from 2 to 4, the conjugation degree of the molecule will increase, resulting in a red shift of the emission wavelength and an enhancement of the fluorescence intensity. The aldehyde group of 2-TPB is located at 2-position, the molecular structure is distorted and the conjugation is limited due to the large steric hindrance, making it difficult for π electrons to delocalize effectively within the whole molecule. Therefore, its energy gap is large, resulting in the emission peak at about 452 nm, and its fluorescence intensity is the lowest due to the large number of nonradiative transition channels. When the substitution site of 3-TPB moved to 3-position, the molecular planarity was improved and the conjugation system was enlarged, so the steric hindrance of the meta-substitution is significantly reduced for the improvement of the degree of torsion planarity, which will make the π-conjugated system extend and the delocalization of π-electrons enhance, leading to an obvious increase of the fluorescence intensity. In addition, the 4-position substitution of 4-TPB makes the molecule more planar for the π–π conjugation, so the para-linkage is an ideal site to make the TPE core and aldehyde group form an effective conjugation system for the π electrons delocalization. Therefore, the emission peak is obviously red-shifted to about 474 nm, and the fluorescence intensity significantly increases with the enhance of radiative transition efficiency. At the same time, 4-TPPB is introduced biphenyl group at the 4-position on the basis of 4-TPB for the expansion of the conjugation system and increase of the molecular rigidity, which reduces the energy gap of the molecule, resulting in the maximum emission peak shift to about 476 nm. On the other hand, the larger conjugation system would enhance the intermolecular rigidity and restrict the intramolecular rotation to suppresses the non-radiative transition, so its fluorescent intensity is the strongest in the series.

The TPB series were further constructed with pyridineacetonitrile to obtain TPE-PY derivatives, which showed the obvious AIE properties with an intramolecular charge transfer (ICT) effect due to the formation of typical D-A-D structure. It is worth noting that TPE-4PY with a 4-position pyridine has an obvious conjugation and ICT effect as compared with TPE-3PY, so its emission wavelength remarkably increased to 517 nm from 436 nm of TPE-3PY. TPE-3PY with the 3-position pyridine has the shortest emission wavelength in this series due to the absence of significant conjugation prolongation. At the same time, the conjugation system of TPE-PPY is further prolonged on the basis of TPE-4PY for the remarkable ICT effect, and the increase of steric hindrance with an additional benzene ring makes the fluorescence intensity enhance due to the restriction of non-radiative decay. This indicates that the excellent luminescence performance is not only due to the unique electronic effects, but also due to the conjugation enhancement with various sites substitutions. Such a synergism profoundly demonstrates the relationship between structure and performance. Moreover, through the precise molecular design, the wavelength and luminescence intensity of the anticipated dyes can be precisely controlled by the adjustment of the substitution sites, conjugation length and donor-acceptor strength to provide important theoretical and experimental basis for the development of new optical materials. This transition was further corroborated by the Commission Internationale de l'Éclairage (CIE) chromaticity diagram in Fig. 1(g). Notably, TPE-2PY, TPE-4PY, and TPE-PPY exhibit a pronounced redshift in their emission peaks, which could be attributed to the expanded π-conjugation system and the electron-withdrawing effect of –C≡N. These factors likely reduce the band gap, facilitating electronic transitions and leading to an increase in emission wavelength. Therefore, the changes in molecular structure, particularly the variety of the substitutions positions and the introduction of the electron-withdrawing groups, are likely the key factors responsible for the variations in the emission wavelengths and intensity of these compounds, which is consistent with the quantum calculation results presented in Fig. 3 below.

The time-resolved emission decay curves with fluorescence lifetimes (h) and correlation coefficients (χ) of TPE-PY, as well as the DVBC, DVBPA monomers, and the PEG-BPA1 copolymer are shown in Fig. 1(h). The fluorescence lifetimes of TPE-PY compounds show significant differences, which directly reflects the profound influence of pyridine substitution sites on the decay efficiency of excited states. The decay curve of TPE-3PY follows a single first-order exponential function with a lifetime of 7.73 ns, being the longest decay life in the series due to the strong fluorescence intensity. The meta-substitution may introduce a unique excited state configuration: its excited state is not a typical strong ICT state, but is closer to a locally excited state (LE) or a twisted ICT state [33, 34]. This geometric constraint leads to the restriction of the internal vibration and rotation of the molecule, which significantly suppresses the nonradiative relaxation channel, so that the system decays in a single radiation path and exhibits a long lifetime. In contrast, the decay curves of TPE-2PY, TPE-4PY and TPE-PPY all need to be fitted by second order exponential functions, indicating that the decay processes of their excited states are more complex, usually involving multiple conformations or relaxation processes at different energy levels. Among them, both TPE-4PY and TPE-PPY are para-connected, which enables the donor and acceptor to form an effective D-A structure, thus establishing a typical ICT channel. Due to the introduction of additional biphenyl groups of TPE-PPY, the conjugation length is extended and the donor ability is enhanced, and the proportion of long-lived components is higher, indicating that the ICT state of the system is more stable and the radiation efficiency is relatively

higher. The fluorescence lifetimes of the intermediate DVBC and monomer DVBPA are not significantly longer than those of the TPE-PY series, and are even slightly shortened than that of TPE-2PY and TPE-3PY, which indicate that the new relaxation channels dominate the decay of the excited state. As an amphiphilic copolymer, PEG-BPA1 self-assembles to form nano-micelles in aqueous solution, and the hydrophobic DVBPA segments are tightly wrapped in the micelle core. The favorable water dispersion makes the energy of excited state migrate through non-radiative quenching channels for a significantly short fluorescence lifetime. As shown in Fig. 1(i), the DPBPA monomer exhibits a distinct absorption peak at approximately 365 nm attributing to the n → π ttransition due to its extended conjugation aromatic system of the multiphenyl units and pyridine rings. After polymerization with PEGMA, the resulting PEG-BPA copolymer shows a slight blue shift of 335 nm with a more distinct absorption peak at 282 nm from the π → π Aelectronic transition. Otherwise, both DPBPA and PEG-BPA exhibit negligible absorption beyond 450 nm from light scattering influence caused by large particles aggregation, indicating good solubility and dispersibility in the solvent.

The images and emission spectra of TPE-4PY under sunlight and UV light after NH_3/HCl vapor fumigation are shown in Figs. 2(a) and 2(b) to investigate its pH sensitivity. Under sunlight, TPE-4PY appears dark yellow, while under UV light, it exhibits a bright yellow-green fluorescence. After HCl vapor fumigation, the color changes to brownish-red under sunlight and bright red under UV light. Subsequently, the color reversibly returns to its original state when exposed to NH_3 vapor again. As shown in the fluorescence spectra in Fig. 2(b), the emission wavelength of TPE-4PY in its initial state (S_1) is approximately 545 nm. However, after HCl vapor exposure, the emission wavelength (F_{a1}) undergoes a redshift to around 640 nm, accompanied by a significant decrease in fluorescence intensity compared to the S1 state. Notably, under alternating NH_3/HCl vapor fumigation, the emission wavelength can reversibly switch between 545 and 640 nm. This phenomenon is attributed to the protonation of the pyridine ring in TPE-4PY under acidic conditions, which may lead to its favorable π-conjugation system and D-A effect for the electron delocalization, so the band gap (ΔE) significantly decreases for the electronic transition energy and the red shift of the emission wavelength.

Figures 2(c) and 2(d) present the fluorescence emission spectra of DVBPA monomer and PEG-BPA1 copolymers in H_2O/THF mixtures with different volume ratios. In pure THF solution, both DVBPA and PEG-BPA1 exhibit weak fluorescence emission, which can be attributed to the fact that the molecules adopt an extended conformation in a good solvent environment to facilitate the intramolecular rotations and vibrations in the excited state, leading to enhanced non-radiative decay pathways and suppressed fluorescence emission. As the water fraction (F_w) gradually increases to 50%, the fluorescence intensity of DVBPA slightly decreases, accompanied by a pronounced red shift in the emission peak, which suggests that the molecule undergoes a transition to a twisted intramolecular charge transfer (TICT) state [35, 36]. In this state, the energy gap between the ground and excited states narrows, which favors non-radiative transitions and leads to fluorescence decreasing. When F_w exceeds 50%, the fluorescence intensity of DVBPA increases significantly and reaches its maximum in F_w of 80%. This enhancement results from the reduced solubility of DVBPA in the mixed solvent system as the water content increases, which induces molecular aggregation to restrict the intramolecular motions (RIM), effectively suppressing

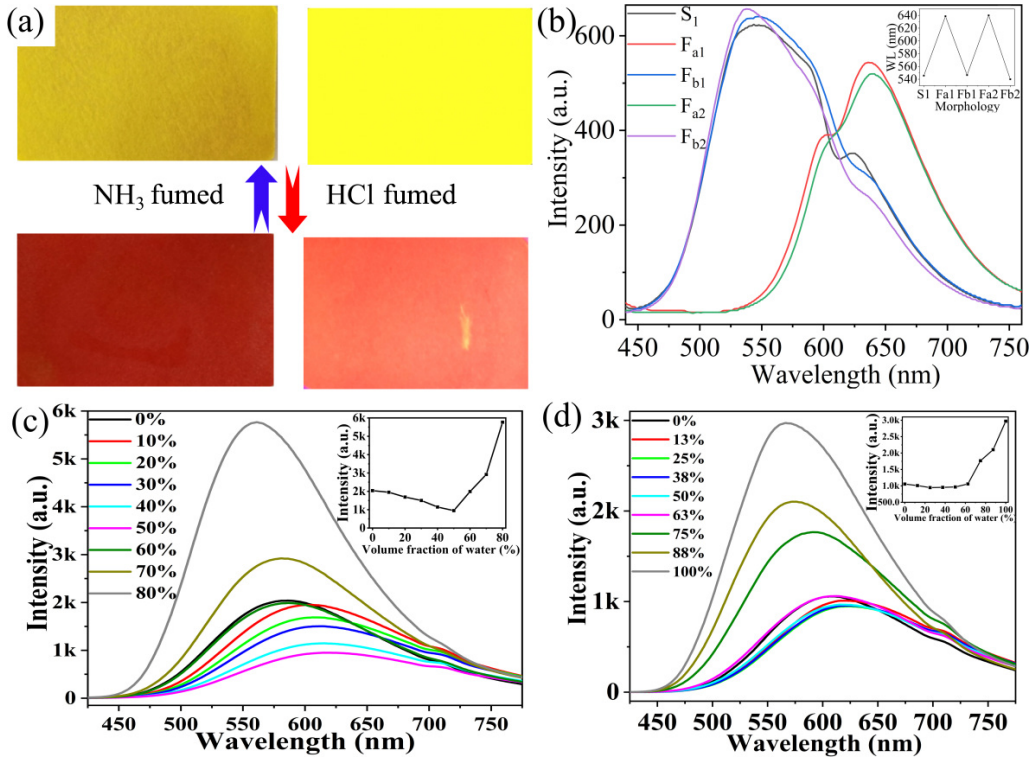

Figure 2 (a) Reversible fluorescence of TPE-4PY dye: samples after HCl/NH_3 fumigation under sunlight (left) and UV light (right). (b) Emission spectra of TPE-4PY: pristine (S_1), after HCl (F_{a1}) and NH_3 (F_{b1}) fumigation, and after secondary fumigation (F_{a2}, F_{b2}). Inset: reversibility of two-photon fluorescence wavelengths. (c) Fluorescence emission of DVBPA monomer in THF/H_2O mixtures with varying volume ratios. (d) Fluorescence emission of PEG-BPA1 copolymers in water solution.

non-radiative decay pathways and thus activating a typical AIE effect [35]. As shown in Fig. 2(d), the PEG-BPA1 copolymer shows relatively stable fluorescence intensity when the F_w was less than 60%, but its overall emission intensity remains lower than that of the DVBPA monomer. This difference likely originates from the introduction of the hydrophilic PEGMA segments, which increase the overall polarity of the polymer and promote the RIM process for the non-radiative decay. Nevertheless, when F_w exceeds 60%, PEG-BPA1 copolymers still exhibits a pronounced AIE behavior, and its fluorescence intensity gradually increases with the degree of aggregation and reaches a maximum in pure water. In order to further study the optical performance of the PEG-BPA1 copolymers, their relationship of fluorescence intensity and particle size is shown in Fig. S8 in the ESM, and the fluorescence intensity gradually increases with the particle size, while the emission wavelength remains nearly constant. This result suggests that larger particle sizes can enhance intermolecular aggregation, thereby improving fluorescence efficiency and exhibiting typical AIE behavior.

3.2 Theoretical calculations of TPE-2PY, TPE-4PY, TPE-PPY and TPE-PPY-H$^+$

To further investigate the influence of structural changes and electrons distribution on fluorescence characteristics, quantum calculations based on frontier molecular orbitals were performed using the B3LYP/6-31+G(d) method of Gaussian 09 for neutral TPE-3PY, TPE-4PY, TPE-PPY, and protonated TPE-PPY. Figure 3 illustrates their highest occupied molecular orbital (HOMO) and lowest unoccupied molecular orbital (LUMO) models, along with the energy band gap ΔE. For neutral TPE-3PY, TPE-4PY and TPE-PPY, the calculated band gaps ΔE are 3.27, 3.11, and 2.98 eV, respectively. These variations of band gaps mainly arise from the effects of substituent positions on molecular conjugation and geometric structure. The 3-substitution in TPE-3PY results in a relatively larger band gap due to weaker conjugation and greater steric hindrance. In contrast, the 4-position substitution in TPE-4PY strengthens the conjugation and D-A effect among the pyridine units, –C≡N group and the TPE units, thereby reducing the band gap. The introduction of a biphenyl group in TPE-PPY further extends the π-conjugation system and enhances electron delocalization, resulting in the smaller band gap among the three compounds.

These findings demonstrate that substituent positions significantly influence the energy distribution of frontier molecular orbitals by modulating molecular conjugation effects and geometric structure, thereby determining the band gap magnitude. Upon protonation, the band gap of TPE-PPY decreases dramatically from 2.98 to 1.10 eV, indicating that the protonation facilitates the electron transition from TPE to pyridine units and significantly reduces the band gap of HOMO and LUMO models due to structural rearrangements via protonation for the enhancement of electron transfer feasibility. Overall, the conjugation effect and various site substitutions on the fluorescence emission spectra discussed earlier, these results further confirm that by adjusting the molecular structures, the fluorescence wavelength variations can be effectively tuned through sites substitutions for the band gap modulation, thereby enabling precise control over fluorescence properties. The redox behaviors of TPE-PY derivatives are further investigated by the cyclic voltammetry (CV) curves as shown in Fig. S9 in the ESM to reveal the influence of the substitution positions and conjugation effect on the electronic structure and electrochemistry property. The energy gap (ΔE) of the oxidation potential and reduction potential is respectively 2.26, 2.42 and 2.12 eV, in other words, TPE-PPY present the lowest energy gap (ΔE) due to the conjugation effect by the introduction of a biphenyl bridge.

3.3 Cytotoxicity and cells imaging of DPT-4PY FONs and PEG-BPA FONs

In the field of biological imaging, the biocompatibility of fluorescent nanoparticles is one of the core factors in determining their potential for application [37–39]. Figures 4(a_1)–4(a_3) present micrographs of A549 cells incubated for 24 h with DPT-4PY FONs at concentrations of 0, 20, and 80 μp/mL. The images reveal that cells morphology basically remains unchanged across all treatment groups as compared to the control, suggesting that DPT-4PY FONs exhibit no significant cytotoxic effects on A549 cells. Figure 4(a_4) shows the cell viability of DPT-4PY FONs assessed by the cell counting kit-8 (CCK-8) method, and it can be observed that, even at a concentration of 120 μg/mL, the cells viability still remains above 95%, indicating that DPT-4PY FONs exhibit excellent biocompatibility.

The pH dynamic regulation mechanism in tumor cells has significant research value in tumor biology. Normally, the pH of

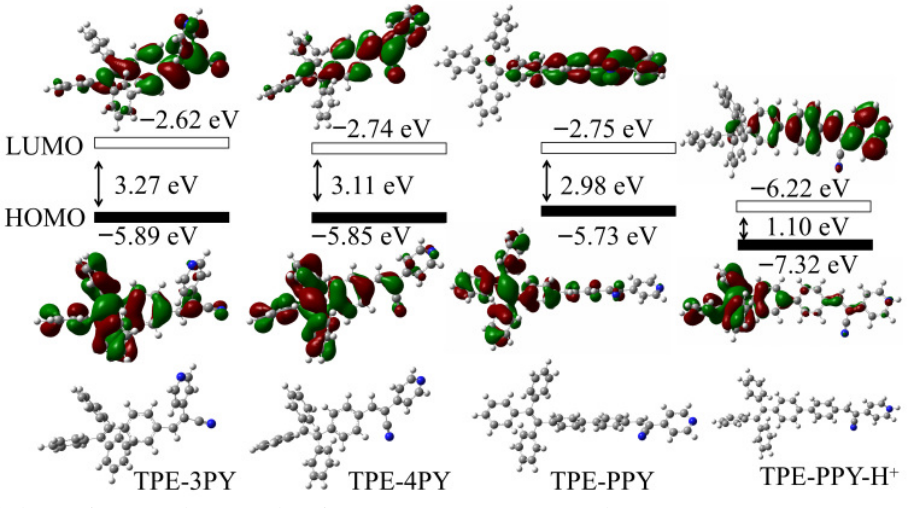

Figure 3 The quantum calculations of LUMO and HOMO orbits of TPE-2PY, TPE-4PY, TPE-PPY, and TPE-PPY-H$^+$.

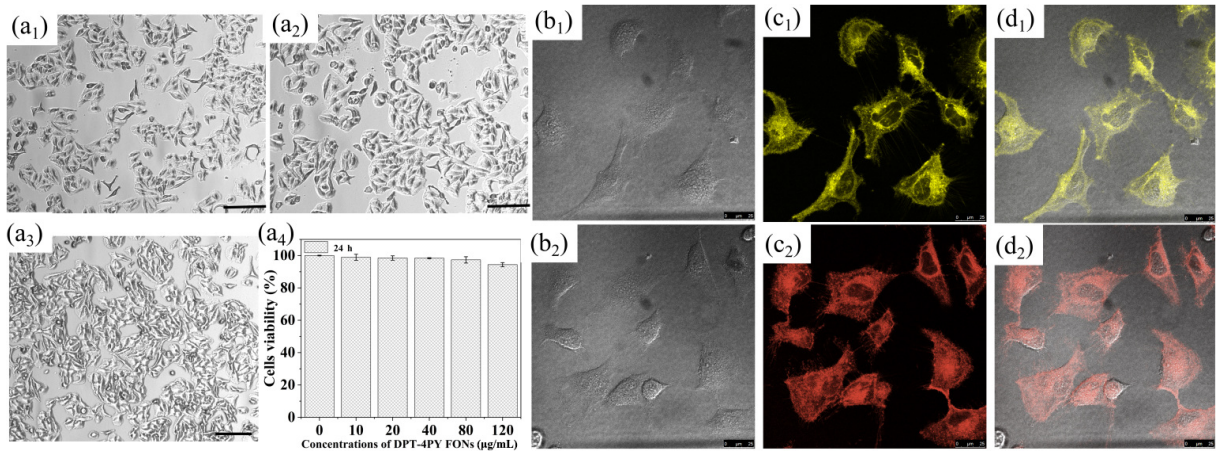

Figure 4 Toxicity assessment of DPT-4PY FONs. Optical images of A549 cells incubated with DPT-4PY FONs of various contents for 24 h: (a_1) control group; (a_2) 20 μg/mL; (a_3) 80 μg/mL, Scale bars =100 μm; (a_4) viability of A549 cells incubated with DPT-4PY FONs of various contents for 24 h. Confocal laser scanning microscope (CLSM) images of A549 cells cultured with 20 μg/mL of DPT-4PY FONs at different pH: (b_1) and (b_2) bright field; (c_1) and (c_2) excited with 405 nm laser; (d_1) and (d_2) combined image of (b_1) and (b_2), and (c_1) and (c_2). (b_1), (c_1), and (d_1), pH = 7.0; (b_2), (c_2), and (d_2), pH = 4.0, Scale bars = 25 μm.

intracellular lysosomes ranges from 4.5 to 5.0, in contrast, the pH within normal cells remains relatively neutral (around 7.2–7.4) [40–44]. This unique pH gradient difference not only reflects the special metabolic and microenvironment adaptation mechanisms of tumor cells but also provides an important biological context for studying the fluorescence behavior changes of fluorescent nanoparticles under different pH conditions. As shown in Figs. 4(b)–4(d), the pH sensitivity of DPT-4PY FONs in A549 cells was investigated via CLSM images under different pH conditions, and it can be observed that DPT-4PY FONs mainly accumulate in the cytoplasm, indicating that DPT-4PY FONs were easily internalized by A549 cells. Additionally, as shown in Fig. 4(c), the cells cultured in different pH media displayed different fluorescence colors. When the pH of the culture medium was 7.0, the fluorescence appeared yellow-green, while at pH 4.0, the fluorescence shifted to orange-red, and these results demonstrate that DPT-4PY FONs hold great potential for applications in tumor cells detection.

The optical images of A549 cells after 24 h incubation with various concentrations of PEG-BPA1 FONs were shown in Fig. S10 in the ESM. Notably, the cellular morphology examination revealed no significant alterations in A549 cells upon treatment with all concentrations of PEG-BPA1 FONs. To further verify the low toxicity and excellent biocompatibility of PEG-BPA1 FONs, the cell viability of A549 cells was evaluated by the CCK-8 method, as shown in Fig. 5(a). The experimental results indicate that PEG-BPA1 FONs have minimal impact on cells viability within the tested concentration range. Even at a concentration as high as 120 μg/mL, the cell viability remained above 95%, fully demonstrating the low toxicity and excellent biocompatibility of PEG-BPA1 FONs.

As shown in Fig. 5(b), PEG-BPA1 FONs exhibited bright orange fluorescence signals in the cytoplasmic region, indicating successful internalization by the cells. The DAPI-stained image clearly showed the cell nuclei marked with blue fluorescence of Fig. 5(c), and it can be observed that the orange fluorescence-labeled PEG-BPA1 FONs are spatially separated from the blue nucleus region as shown in Fig. 5(d), also suggesting that PEG-BPA1 FONs primarily localize at the cytoplasm and do not undergo significant nuclear transport. The fluorescence overlay image of Fig. 5(e) visually presented the relative positions of PEG-BPA1 FONs and the cell nuclei stained by DAPI. To quantitatively characterize the distribution patterns, Fig. 5(f) provides a quantitative analysis of the intracellular distribution of PEG-BPA1 FONs and DAPI, indicating that PEG-BPA1 FONs were effectively internalized and predominantly distributed in the cytoplasm.

3.4 Drug release and anti-tumor effect of BPA-PTX FONs

PTX is a potent anticancer drug that can inhibit tumor cells growth, however, its biological application is limited by its poor aqueous solubility and reduced systemic bioavailability [45–48]. To overcome these issues, PTX can be combined with amphiphilic fluorescent nanoparticles, which not only improve the solubility and targeting ability of PTX but also enable real-time tracking of drug release through their fluorescence emission, so the copolymers PEG-BPA are used as a carrier of PTX for BPA-PTX FONs by self-assembly of PEG-BPA and PTX to evaluate their anti-tumor effects *in vitro*. In this self-assembled system, the hydrophobic DVBPA components effectively encapsulated PTX molecules, while the hydrophilic PEG segments formed a stabilizing outer shell to enhance the dispersion of BPA-PTX FONs in aqueous media and protect them from degradation or inactivation caused by external environmental factors. As shown in the TEM image in Fig. 6(a), BPA-PTX FONs exhibited a uniform spherical morphology with particle sizes ranging from 200–300 nm, which were well dispersed in aqueous solution.

To further evaluate the release behavior of BPA-PTX FONs, a drug release study of PTX was conducted *in vitro* under different pH conditions using a dialysis method [49]. A calibration curve of PTX in CH_3OH was first established, and the released PTX was quantified by UV spectroscopy. As illustrated in Fig. 6(b), the cumulative release percentages of PTX over 48 h were measured in PBS buffer solutions at pH 7.4 of physiological conditions and pH 5.1 of mildly acidic conditions for the tumor microenvironment, and the analysis results showed a cumulative release rate of 47.0% at pH 7.4 and a slightly higher rate of 73.5% at pH 5.1, indicative of the pH-responsivity of BPA-PTX FONs for the drug release, which was suitable for tumor cells inhibition. According to calculations based on Eqs. (1) and (2), the encapsulation efficiency (EE%) and drugs-loaded content (LC%) of BPA-PTX FONs were about 87.4% and 21.8%.

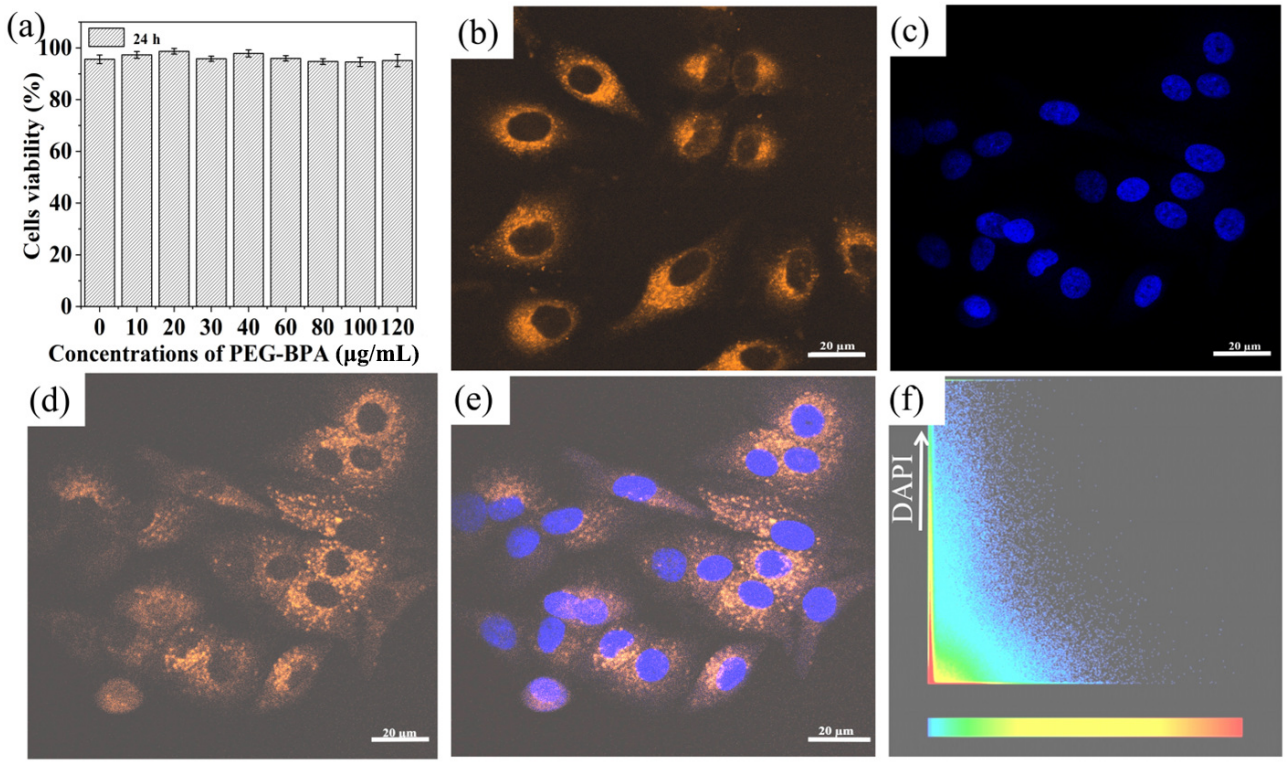

Figure 5 (a) Cell survival rate following 24 h exposure to different doses of PEG-BPA1 FONs. Cellular uptake and localization are displayed in (b)–(e): (b) intrinsic fluorescence of PEG-BPA1 FONs (20 μg/mL), (c) nuclear staining by DAPI, (d) PEG-BPA1 channel, and (e) the corresponding merged image. Scale bars = 20 μm. (f) Quantification of fluorescence distribution for both DAPI and PEG-BPA1 FONs in the cells.

$$EE\% = \frac{\text{Amount of PTX in NPs}}{\text{Total amount of PTX added}} \times 100\% \quad (1)$$

$$LC\% = \frac{\text{Amount of PTX in NPs}}{\text{NP's weight}} \times 100\% \quad (2)$$

The cellular morphology of A549 cells with various concentrations of BPA-PTX FONs was presented in Fig. S11 in the ESM, and the cells morphology changed from oval to round with the increase of the concentration as compared with the control group, indicating that BPA-PTX FONs exert an inhibitory effect on A549 tumor cells. The cells viability was studied using the CCK-8 method as shown in Fig. 6(c), and it can be seen that the cells survival rate decreased significantly to 23.7% with the increase of BPA-PTX FONs concentration, confirming that PTX was successfully delivered to A549 cells for the expected inhibitory effect of BPA-PTX FONs on tumor cells. The CLSM image of A549 cells with 20 μg/mL BPA-PTX FONs was shown in Figs. 6(d) and 6(e), and the BPA-PTX FONs exhibited orange fluorescence in the cytoplasm, indicating effective uptake by the A549 cells and localization in the cytoplasm. The CLSM image of A549 cells stained with BPA-PTX FONs and DAPI was shown in Figs. 6(f)–6(h), where the orange fluorescence signal of BPA-PTX FONs is mainly distributed in the cytoplasm with the blue fluorescence signal at the nuclei, also indicating that BPA-PTX FONs mainly located at the cytoplasm. The quantitative analysis of the fluorescence distribution of DAPI and BPA-PTX FONs was demonstrated Fig. 6(i), systematically revealing the intracellular distribution pattern of BPA-PTX FONs. In summary, the prepared BPA-PTX FONs are efficiently taken up by A549 cells and are primarily localized at the cytoplasm with a significant cytotoxicity, which indicate that this platform has broad application prospects in bioimaging, drug delivery systems and tumor-targeted therapy.

4 Conclusions

In conclusion, a series of fluorescent materials with AIE properties with multi-site substitutions were constructed through molecular structure regulation. Firstly, TPB and TPE-PY derivatives with different substitution sites were designed and synthesized to explore the effect of substitution positions on photophysical properties, and TPE-PY showed typical AIE behavior and good responsiveness to environmental pH, demonstrating its application potential as a fluorescent probe for the tumor microenvironment. On this basis, the amphiphilic copolymers PEG-BPA were prepared by RAFT polymerization of DVBPA monomers with AIE activity, which can self-assemble in aqueous solution to form fluorescently stable PEG-BPA FONs with 100–200 nm diameter, and their co-incubation experiments with A549 cells showed that the cells survival rate was more than 95%, indicative of the low toxicity and excellent biocompatibility. Moreover, the drug-loaded system of BPA-PTX FONs from the self-assembly of PEG-BPA and PTX had high drug loading efficiency of 21.8% and cumulative release rate of 73.5%, which could be absorbed by A549 cells with excellent inhibition rate of 23.7%.

Finally, this study has proposed a construction strategy combining AIE molecular design with amphiphilic copolymers self-assembly, and successfully developed a multifunctional nanoplatform with both fluorescence imaging and drug delivery functions. The system not only shows broad application prospects in tumor targeted therapy and visualization of drug release, but also

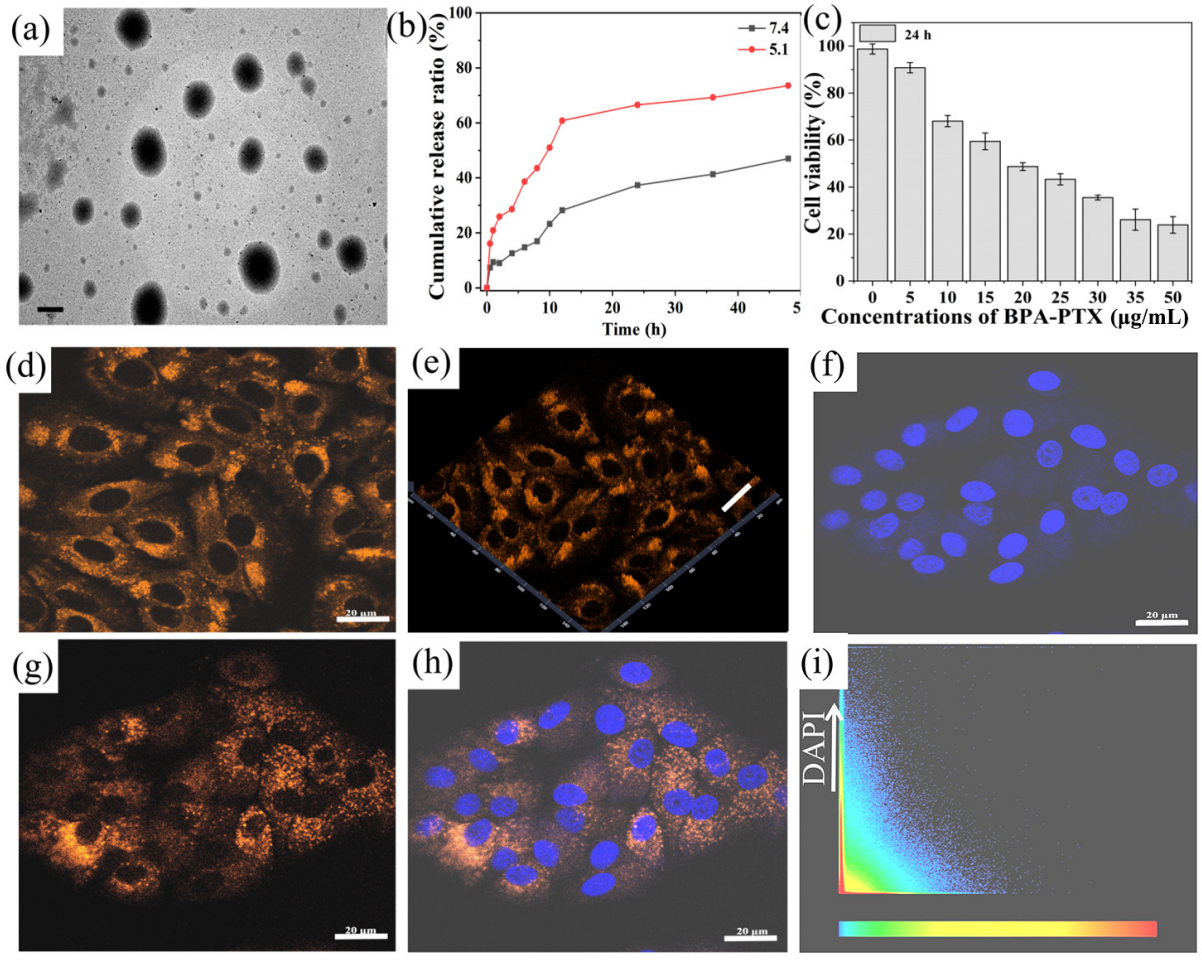

Figure 6 (a) TEM image of BPA-PTX FONs dispersing in water, scale bar = 200 nm. (b) Cumulative release of PTX from BPA-PTX FONs at 37 °C under various pH conditions. (c) Cell viability of A549 cells after 24 h incubation with different concentrations of BPA-PTX FONs. Cellular imaging of A549 cells treated with 20 μg/mL BPA-PTX FONs: (d) BPA-PTX channel (without DAPI); (e) 2.5 D image of (d); (f) DAPI channel (nuclei); (g) BPA-PTX with DAPI; (h) merge of (f) and (g); scale bars = 20 μm. (i) Quantification of fluorescence distribution for DAPI and BPA-PTX FONs in cells.

provides strong support for the design of new fluorescent functional materials and the construction of multifunctional nano-drug delivery systems.

Electronic Supplementary Material: Supplementary material (materials and characterization, synthesis of TPB, TPE-PY derivatives and DVBPA monomers with their mass spectra, fabrication of PEG-BPA copolymers, DPT-4PY FONs and BPA-PTX FONs, deliver and release of PTX, particle size-fluorescence relationship, and cytotoxicity evaluation images) is available in the online version of this article at https://doi.org/10.26599/NR.2026.94908481.

Data availability

All data needed to support the conclusions in the paper are presented in the manuscript and/or the Electronic Supplementary Material. Additional data related to this paper may be requested from the corresponding author upon request.

Acknowledgements

This research was supported by Guangdong Province via the College and University Projects (No. 2023ZDZX3043) and the Quality Engineering Program (No. SKJ202302), and the Climbing Plan (No. pdjh2024b429). Z. F. H. thanks the Department of Chemistry for providing opportunity of Visiting Scholarship at Tsinghua University.

Declaration of competing interest

All the contributing authors report no conflict of interests in this work.

Author contribution statement

Z. F. H.: Writing – original draft, writing – review & editing, investigation, software, methodology, conceptualization. J. W. T.: Writing – original draft, investigation, data curation. S. Y. Y.: Investigation. W. C. Z.: Investigation. J. T. Z.: Investigation. Y. Y.: Supervision. M. T.: Supervision. J. Y. Y.: Writing – review & editing, supervision. L. T.: Writing – review & editing, supervision. Y. W.: Writing – review & editing, supervision. All the authors have approved the final manuscript.

Informed consent

Not applicable.

Ethics statement

Not applicable.

Use of AI statement

None.

References

[1] Wang, J. Q.; Zhang, L. Y.; Li, Z. Aggregation-induced emission luminogens with photoresponsive behaviors for biomedical applications. *Adv. Healthc. Mater.* **2021**, *10*, 2101169.

[2] Wang, Y.; Xia, K.; Wang, L. C.; Wu, M. X.; Sang, X. J.; Wan, K. M.; Zhang, X. D.; Liu, X. M.; Wei, G. Peptide-Engineered fluorescent nanomaterials: Structure design, function tailoring, and biomedical applications. *Small* **2021**, *17*, 2005578.

[3] Zheng, M.; Wang, Y. L.; Zhang, D. T.; Zhu, M. Q. Fluorescent materials with excellent biocompatibility and their application in bio-sensing, bio-imaging. *Biosensors* **2023**, *13*, 906.

[4] Qiu, Z. J.; Liu, X. L.; Lam, J. W. Y.; Tang, B. Z. The marriage of aggregation-induced emission with polymer science. *Macromol. Rapid Commun.* **2019**, *40*, 1800568.

[5] Mei, J.; Hong, Y. N.; Lam, J. W. Y.; Qin, A. J.; Tang, Y. H.; Tang, B. Z. Aggregation-Induced emission: The whole is more brilliant than the parts. *Adv. Mater.* **2014**, *26*, 5429–5479.

[6] He, Z. K.; Ke, C. Q.; Tang, B. Z. Journey of aggregation-induced emission research. *ACS Omega* **2018**, *3*, 3267–3277.

[7] Yang, Z. Y.; Chi, Z. H.; Mao, Z.; Zhang, Y.; Liu, S. W.; Zhao, J.; Aldred, M. P.; Chi, Z. G. Recent advances in mechano-responsive luminescence of tetraphenylethylene derivatives with aggregation-induced emission properties. *Mater. Chem. Front.* **2018**, *2*, 861–890.

[8] Cai, X. L.; Liu, B. Aggregation-Induced emission: Recent advances in materials and biomedical applications. *Angew. Chem., Int. Ed.* **2020**, *59*, 9868–9886.

[9] Chen, S. H.; Xu, J. M.; Li, Y. M.; Peng, B. R.; Luo, L. Y.; Feng, H. Y.; Chen, Z. H.; Wang, Z. Y. Research progress of aggregation-caused quenching (ACQ) to aggregation-induced emission (AIE) transformation based on organic small molecules. *Chin. J. Org. Chem.* **2022**, *42*, 1651–1666.

[10] Guo, M. C.; Song, H.; Li, K.; Ma, M. C.; Liu, Y.; Fu, Q.; He, Z. G. A new approach to developing diagnostics and therapeutics: Aggregation-induced emission-based fluorescence turn-on. *Med. Res. Rev.* **2020**, *40*, 27–53.

[11] Li, C. C.; Shi, X. T.; Zhang, X. D. Clustering-triggered emission of EPS-605 nanoparticles and their application in biosensing. *Polymers* **2022**, *14*, 4050.

[12] Wei, W. C.; Qiu, Z. J. Diagnostics and theranostics of central nervous system diseases based on aggregation-induced emission luminogens. *Biosens. Bioelectron.* **2022**, *217*, 114670.

[13] Luo, F.; Shen, L. Y.; Zhang, J. J.; Huang, Y. L.; Chen, T. X.; Xu, H.; Zhang, Q. L.; Redshaw, C.; Feng, X. Nanoarchitectonics of the aggregation-induced emission luminescent molecule Tetraphenylethylene-COOH (TPE-COOH): Fluorescence imaging of targeted cancer microsphere cells. *Dyes Pigm.* **2023**, *214*, 111192.

[14] Zhang, T. T.; Huang, Y.; Chen, X. Q.; Zheng, F. M.; Shen, Y. T.; Chen, G. Z.; Ye, Q. H.; Chen, K. Z.; Xiao, X. F.; Peng, Y. R. Tetraphenylethylene-Based AIE nanoprobes for labeling lysosome by two-photon imaging in living cells. *Spectrochim. Acta Part A: Mol. Biomol. Spectrosc.* **2024**, *306*, 123630.

[15] Çapan, İ.; Hawash, M.; Jaradat, N.; Sert, Y.; Servi, R.; Koca, İ. Design, synthesis, molecular docking and biological evaluation of new carbazole derivatives as anticancer, and antioxidant agents. *BMC Chem.* **2023**, *17*, 60.

[16] Chan, C. M.; Gao, H.; Wu, J. W.; Li, J.; Tian, J. W.; Xue, Z. L. AIE-active large stokes-shift bodipy functionalized with carbazolyl for lysosome-targeted imaging in living cells. *Spectrochim. Acta Part A: Mol. Biomol. Spectrosc.* **2024**, *323*, 124933.

[17] Lee, K. W.; Gao, Y. J.; Wei, W. C.; Tan, J. H.; Wan, Y. P.; Feng, Z.; Zhang, Y. H.; Liu, Y.; Zheng, X. L.; Cao, C. et al. Anti-Quenching NIR-II J-aggregates of benzo[c]thiophene fluorophore for highly efficient bioimaging and phototheranostics. *Adv. Mater.* **2023**, *35*, 2211632.

[18] Tan, Y. H.; Sun, Y.; Huang, W. G.; Zhu, D. X.; Yan, D. Y.; Wang, D.; Tang, B. Z. Thiophene π-Bridge-Based second near-infrared luminogens with aggregation-induced emission for biomedical applications. *Luminescence* **2024**, *39*, e4606.

[19] La, D. D.; Bhosale, S. V.; Jones, L. A.; Bhosale, S. V. Tetraphenylethylene-based AIE-active probes for sensing applications. *ACS Appl. Mater. Interfaces* **2018**, *10*, 12189–12216.

[20] Feng, H. T.; Yuan, Y. X.; Xiong, J. B.; Zheng, Y. S.; Tang, B. Z. Macrocycles and cages based on tetraphenylethylene with aggregation-induced emission effect. *Chem. Soc. Rev.* **2018**, *47*, 7452–7476.

[21] Chen, S. X.; Qiu, R. M.; Yu, Q. H.; Zhang, X. Y.; Wei, M.; Dai, Z. Y. Boranil dyes bearing tetraphenylethene: Synthesis, AIE/AIEE effect properties, pH sensitive properties and application in live cell imaging. *Tetrahedron Lett.* **2018**, *59*, 2671–2678.

[22] Yang, X. Q.; Xu, C. H.; Zhang, X.; Li, P.; Sun, F. Y.; Liu, X. Y.; Wang, X. Y.; Kwok, R. T. K.; Yang, J. L.; Lam, J. W. Y. et al. Development of sulfonamide-functionalized charge-reversal AIE photosensitizers for precise photodynamic therapy in the acidic tumor microenvironment. *Adv. Funct. Mater.* **2023**, *33*, 2300746.

[23] Jin, Y. X.; Jiang, B. L.; Song, H. J.; Mei, C. M.; Liu, Z. A.; Zhang, X. K.; Liu, J. Y.; Gong, Y. Y. Monophenyl luminescent material with dual-state emission and pH sensitivity for cell imaging. *RSC Adv.* **2024**, *14*, 10942–10952.

[24] Li, S. Y.; Li, K. X.; Gong, X. F.; Yan, P. F.; Sun, S. P. pH-Induced color changeable AIE-featured polymeric micelles for self-indicating anticancer drug delivery. *Sens. Actuators B: Chem.* **2025**, *422*, 136637

[25] Yang, L. L.; Gu, P. L.; Fu, A. X.; Xi, Y. B.; Cui, S. L.; Ji, L. G.; Li, L. L.; Ma, N. N.; Wang, Q. Z.; He, G. J. TPE-based fluorescent probe for dual channel imaging of pH/viscosity and selective visualization of cancer cells and tissues. *Talanta* **2023**, *265*, 124862.

[26] Bernabeu, E.; Cagel, M.; Lagomarsino, E.; Moretton, M.; Chiappetta, D. A. Paclitaxel: What has been done and the challenges remain ahead. *Int. J. Pharm.* **2017**, *526*, 474–495.

[27] Gallego-Jara, J.; Lozano-Terol, G.; Sola-Martínez, R. A.; Cánovas-Díaz, M.; de Diego Puente, T. A compressive review about Taxol®: History and future challenges. *Molecules* **2020**, *25*, 5986.

[28] Zhu, L. W.; Wang, Y. M.; Song, J. Y.; Sheng, Z. H.; Qi, J.; Li, Y.; Li, G. X.; Tang, B. Z. Two-photon absorption aggregation-induced emission luminogen/paclitaxel nanoparticles for cancer theranostics. *ACS Appl. Mater. Interfaces* **2024**, *16*, 27075–27086.

[29] Huang, Z. F.; Zhou, C. Y.; Zhang, X. T.; Xue, H. Y.; Liao, W. X.; Mao, L. C.; Yuan, J. Y.; Tao, L.; Wei, Y. Polymerizable aggregation-induced emission enhancement (AEE) dyes with D-A-D' structure basing on phenothiazine and tetraphenylethylene for fluorescent particles and their application in cell imaging. *Eur. Polym. J.* **2025**, *223*, 113643.

[30] Tao, L.; Liu, J. Q.; Davis, T. P. Branched polymer-protein conjugates made from mid-chain-functional p(HPMA). *Biomacromolecules* **2009**, *10*, 2847–2851.

[31] Huang, Z. F.; Chen, Y. L.; Zhou, C. Y.; Wang, K.; Liu, X. B.; Mao, L. C.; Yuan, J. Y.; Tao, L.; Wei, Y. Amphiphilic AIE-active copolymers with optical activity by chemoenzymatic transesterification and RAFT polymerization: Synthesis, self-assembly and biological imaging. *Dyes Pigm.* **2021**, *184*, 108829.

[32] Huang, Z. F.; Li, Q. S.; Xue, H. Y.; Liao, W. X.; Feng, Y. Q.; Yuan, J. Y.; Tao, L.; Wei, Y. Synthesis of an aggregation-induced emission (AIE) dye with pH-sensitivity based on tetraphenylethylene-pyridine for fluorescent nanoparticles and its applications in bioimaging and *in*

vitro anti-tumor effect. *Colloids Surf. B: Biointerfaces* **2024**, *234*, 113750.
[33] Suzuki, K.; Sakuda, E.; Tani, Y.; Akiyama, M.; Albrecht, K.; Aizawa, N.; Izawa, S.; Kaji, H. Dynamic excitons in organic light-emitting systems. *J. Chem. Phys.* **2025**, *162*, 061001.
[34] Lin, Z. S.; Ye, J. T.; Shinohara, S.; Tanaka, Y.; Yoshioka, R.; Chan, C. Y.; Lee, Y. T.; Tang, X.; Mitrofanov, K.; Wang, K. et al. Blue organic long-persistent luminescence via upconversion from charge-transfer to locally excited singlet state. *Nat. Commun.* **2025**, *16*, 2686.
[35] Xu, N.; Qiao, Q. L.; Liu, X. G.; Xu, Z. C. Enhancing brightness and photostability of organic small molecular fluorescent dyes through inhibiting twisted intramolecular charge transfer (TICT). *Acta Chim. Sin.* **2022**, *80*, 553–562.
[36] Zhang, W.; Kong, J.; Miao, R.; Song, H. W.; Ma, Y. L.; Zhou, M.; Fang, Y. Integrating aggregation induced emission and twisted intramolecular charge transfer via molecular engineering. *Adv. Funct. Mater.* **2024**, *34*, 2311404.
[37] Kumar, K. S. S.; Girish, Y. R.; Ashrafizadeh, M.; Mirzaei, S.; Rakesh, K. P.; Gholami, M. H.; Zabolian, A.; Hushmandi, K.; Orive, G.; Kadumudi, F. B. et al. AIE-Featured tetraphenylethylene nanoarchitectures in biomedical application: Bioimaging, drug delivery and disease treatment. *Coord. Chem. Rev.* **2021**, *447*, 214135.
[38] Ou, Y. C.; Wang, X. F.; He, N.; Wang, X.; Lu, D.; Li, Z.; Luo, F.; Li, J. H.; Tan, H. A biocompatible polyurethane fluorescent emulsion with aggregation-induced emission for targeted tumor imaging. *J. Mater. Chem. B* **2023**, *11*, 2266–2275.
[39] Wang, N.; Zhou, Q.; Luo, X. L.; Zhang, Y. M.; Li, K.; Yu, X. Q. A facile strategy to construct biocompatible fluorescent nanoparticles for intracellular bioimaging. *Polymer* **2024**, *290*, 126486.
[40] Bogdanov, A.; Bogdanov, A.; Chubenko, V.; Volkov, N.; Moiseenko, F.; Moiseyenko, V. Tumor acidity: From hallmark of cancer to target of treatment. *Front. Oncol.* **2022**, *12*, 979154.
[41] Chu, S. L.; Shi, X. L.; Tian, Y.; Gao, F. X. pH-responsive polymer nanomaterials for tumor therapy. *Front. Oncol*. **2022**, *12*, 855019.
[42] Ohkuma, S.; Poole, B. Fluorescence probe measurement of the intralysosomal pH in living cells and the perturbation of pH by various agents. *Proc. Natl. Acad. Sci. USA* **1978**, *75*, 3327–3331.
[43] Sun, H. L.; Li, X. Y.; Liu, Q.; Sheng, H. G.; Zhu, L. Q. pH-responsive self-assembled nanoparticles for tumor-targeted drug delivery. *J. Drug Target.* **2024**, *32*, 672–706
[44] Zhang, Z. C.; Ding, C. W.; Sun, T. D.; Wang, L.; Chen, C. X. Tumor therapy strategies based on microenvironment-specific responsive nanomaterials. *Adv. Healthc. Mater.* **2023**, *12*, 2300153.
[45] Ramezanpour, A.; Ansari, L.; Rahimkhoei, V.; Sharifi, S.; Bigham, A.; Lighvan, Z. M.; Rezaie, J.; Szafert, S.; Mahdavinia, G.; Akbari, A. et al. Recent advances in carbohydrate-based paclitaxel delivery systems. *Polym. Bull.* **2024**, *81*, 1043–1069.
[46] Bawankule, A. K.; Tatode, A. A.; Patil, P. S.; Umekar, M. J. Folate-mediated paclitaxel nanodelivery systems: A comprehensive review. *Turk. J. Pharm. Sci.* **2023**, *20*, 58–67.
[47] Mustafa, G.; Hassan, D.; Ruiz-Pulido, G.; Pourmadadi, M.; Eshaghi, M. M.; Behzadmehr, R.; Tehrani, F. S.; Rahdar, A.; Medina, D. I.; Pandey, S. Nanoscale drug delivery systems for cancer therapy using paclitaxel-A review of challenges and latest progressions. *J. Drug Deliv. Sci. Technol.* **2023**, *84*, 104494.
[48] Sati, P.; Sharma, E.; Dhyani, P.; Attri, D. C.; Rana, R.; Kiyekbayeva, L.; Büsselberg, D.; Samuel, S. M.; Sharifi-Rad, J. Paclitaxel and its semi-synthetic derivatives: Comprehensive insights into chemical structure, mechanisms of action, and anticancer properties. *Eur. J. Med. Res.* **2024**, *29*, 90.
[49] Wang, Z. Y.; Wang, C.; Fang, Y. Y.; Yuan, H.; Quan, Y. W.; Cheng, Y. X. Color-tunable AIE-active conjugated polymer nanoparticles as drug carriers for self-indicating cancer therapy via intramolecular FRET mechanism. *Polym. Chem.* **2018**, *9*, 3205–3214.